Banks of templates for directed searches of gravitational waves from spinning nuetron stars

Andrzej Pisarski,* Piotr Jaranowski,† and Maciej Pietka‡
Faculty of Physics, University of Białystok, Lipowa 41, 15–424 Białystok, Poland
(Dated: October 15, 2010)

We construct efficient banks of templates suitable for directed searches of almost monochromatic gravitational waves originating from spinning nuetron stars in our Galaxy in data being collected by currently operating interferometric detectors. We thus assume that the position of the gravitational-wave source in the sky is known, but we do not assume that the wave's frequency and its derivatives are a priori known. In the construction we employ simplified model of the signal with constant amplitude and phase which is a polynomial function of time. All our template banks enable usage of the fast Fourier transform algorithm in the computation of the maximum-likelihood $\mathcal{F}$-statistic for nodes of the grids defining the bank. We study and employ the dependence of the grid's construction on the choice of the position of the observational interval with respect to the origin of time axis. We also study the usage of the fast Fourier transform algorithms with non-standard frequency resolutions achieved by zero padding or folding the data. In the case of the gravitational-wave signal with one spindown parameter included we have found grids with covering thicknesses which are only 0.1%–16% larger than the thickness of the optimal two-dimensional hexagonal covering.

PACS numbers: 95.55.Ym, 04.80.Nn, 95.75.Pq, 97.60.Gb

I. INTRODUCTION AND SUMMARY

Rotating neutron stars in our Galaxy are expected sources of almost monochromatic gravitational waves which are looked for in the data being collected by currently operating ground-based interferometric detectors LIGO [1], Virgo [2], GEO600 [3], and TAMA [4]. In the present paper we consider the problem of construction of efficient banks of templates needed to detect gravitational-wave signals originating from spinning neutron stars. We assume that the problem of detection of the signal and of estimation of its parameters is based on the *maximum-likelihood* (ML) principle and we also assume that the noise in the detector is Gaussian and stationary (the detailed exposition of the ML detection in Gaussian noise can be found e.g. in Chapter 6 of the monograph [5], see also [6] and the review article [7]). Data analysis tools and algorithms needed to perform, within the ML approach, an *all-sky* search for almost monochromatic gravitational-wave signals (i.e. the search which assumes that the position of the source in the sky is not known) were developed in detail in the series of papers [8–12] (see also Refs. [13, 14]). In our paper we restrict ourselves to *directed* searches for almost monochromatic signals, i.e. we assume that the position of the source in the sky is known. We do not assume however that the frequency and the spindown parameters of the gravitational-wave signal are known. Directed searches should thus be distinguished from *targeted* searches, in which it is additionally assumed that the frequency and the spindown parameters of the gravitational wave are also known (see Refs. [15, 16] for discussions of statistics by means of which one can test whether data contains such signal). Several targeted searches were already performed with data collected by the LIGO and GEO600 detectors [17–21].

In the ML approach one considers the likelihood ratio $\Lambda[x;\boldsymbol{\theta}]$ which is a function of the data x and the parameters $\boldsymbol{\theta}$ of the gravitational-wave signal we are looking for. Detection of the signal relies on the computation of $\Lambda[x;\boldsymbol{\theta}]$ maximized over all possible values of the parameters $\boldsymbol{\theta}$ and comparing this maximum with a threshold. In the case of directed searches the unknown parameters $\boldsymbol{\theta}$ can be divided into two groups, $\boldsymbol{\theta} = (\mathbf{A}, \boldsymbol{\xi})$. The first group $\mathbf{A}$ consists of four *extrinsic* or *amplitude* parameters: an overall amplitude of the waveform, its initial phase, the polarization angle of the wave, and the inclination angle of the star's rotation axis with respect to the line of sight. The second group $\boldsymbol{\xi}$ contains *intrinsic* or *phase* parameters: the frequency of the wave and the spindown parameters. Maximization of the Λ with respect to amplitude parameters $\mathbf{A}$ can be done analytically (by solving the set of ML equations $\partial\Lambda/\partial\mathbf{A} = 0$ with respect to $\mathbf{A}$) and the *$\mathcal{F}$-statistic* is defined as the logarithm of the likelihood ratio Λ after replacing in Λ the amplitude parameters $\mathbf{A}$ by their ML estimators $\hat{\mathbf{A}}$: $\mathcal{F}[x;\boldsymbol{\xi}] := \ln\Lambda[x;\hat{\mathbf{A}},\boldsymbol{\xi}]$. Maximization of the $\mathcal{F}$-statistic over the phase parameters $\boldsymbol{\xi}$ can be done only numerically. To find this maximum one needs to construct a *bank of templates* in the space of the parameters $\boldsymbol{\xi}$ on which the $\mathcal{F}$-statistic depends. The bank of templates is defined by a discrete set of points, i.e. a *grid* in the parameter space chosen in such a way, that for any possible signal there exists a grid point such that the expectation value of the $\mathcal{F}$-statistic (which is a random variable as it depends on the detector's noise which is a stochastic process) computed for the parameters of this grid point

* andrzej@alpha.uwb.edu.pl
† pio@alpha.uwb.edu.pl
‡ map@alpha.uwb.edu.pl

is not less than a certain fixed minimal value (assuming that the minimal value of the signal-to-nise ratio is also a priori fixed).

In the series of papers [8–12] it was argued and checked by numerical simulations that in the case of an all-sky search in the construction of the bank of templates one can employ a simplified model of the gravitational-wave signal, the so called *linear phase model*, in which the amplitude of the signal is assumed to be constant and the signal's phase is a linear function of the unknown parameters (this model was introduced in Sec. V B of Ref. [9]). In Sec. V E of [9] it was checked that the linear model reproduces well the covariance matrix (defined as the inverse of the Fisher matrix) for the ML estimators of the signal's parameters of the exact gravitational-wave signal. Also in Ref. [9] (Sec. V D and Appendix C there) the *polynomial phase model* was introduced in which the signal's amplitude is constant and the phase is a polynomial function of time. It was found (in Sec. V E of [9]) that the polynomial phase model reproduces very well the covariance matrix of the signal's parameters of the exact model in the case of directed searches. This indicates that the polynomial model can be used in the construction of the banks of templates for directed searches and this model is accepted in the present paper.

In the current paper we assume that the observational interval is of the form $\langle t_{\rm i}-T_{\rm o}/2;\, t_{\rm i}+T_{\rm o}/2\rangle$ (where $T_{\rm o}$ is the length of observation time), and we study the dependence of the construction of banks of templates on the choice of the parameter $t_{\rm i}$ (or its dimensionless version $\chi_{\rm i} := t_{\rm i}/T_{\rm o}$) which fixes the position of the observational interval with respect to the origin of time axis.

The organization and the main results achieved in the paper are as follows. In Sec. II we introduce the polynomial phase model of the gravitational-wave signal. We consider here the phase with only one spindown parameter included. For this model we compute the $\mathcal{F}$-statistic and its expectation value in the case when the data contains the gravitational-wave signal. This expectation value depends [see the crucial Eq. (2.33) below] on the signal-to-noise ratio ρ and on the value of the *autocovariance function* $C_0(\boldsymbol{\xi}, \boldsymbol{\xi}')$ of the $\mathcal{F}$-statistic (the subscript '0' indicates that the autocovariance is calculated in the case when data is a pure noise) computed for the intrinsic parameters of the template ($\boldsymbol{\xi}$) and the gravitational-wave signal ($\boldsymbol{\xi}'$), respectively. The signal-to-noise ratio ρ we can not control, therefore to construct bank of templates one needs to choose some minimum value $C_{\rm min}$ of the autocovariance function C_0 and look for such a grid of points that for any point $\boldsymbol{\xi}'$ in the intrinsic parameter space there exists a grid node $\boldsymbol{\xi}$ such that the autocovariance $C_0(\boldsymbol{\xi}, \boldsymbol{\xi}')$ computed for the parameters $\boldsymbol{\xi}$ and $\boldsymbol{\xi}'$ is not less than $C_{\rm min}$. The autocovariance $C_0(\boldsymbol{\tau})$ (for polynomial phase model it depends on $\boldsymbol{\xi}$, $\boldsymbol{\xi}'$ only through the difference $\boldsymbol{\tau} := \boldsymbol{\xi} - \boldsymbol{\xi}'$) can be expressed in terms of Fresnel integrals or one can use an approximate formula for C_0 by taking the Taylor expansion (up to the second-order terms) of C_0 around its maximum at $\boldsymbol{\tau} = \mathbf{0}$. In Fig. 1 and Table I we compare these two ways of computing the autocovariance.

In Sec. III we consider banks of templates necessary to perform detection of almost monochromatic gravitational-wave signals with polynomial phase. We first formulate the problem of constructing bank of templates as a problem of finding optimal covering of the signal's parameter space by means of identical ellipses (defined as isoheights of the autocovariance function C_0 of the $\mathcal{F}$-statistic) and introduce some mathematical notions related with coverings. We are interested in such searches for almost periodic gravitational-wave signals for which the number of grid points in the parameter space is very large and the time needed to compute the $\mathcal{F}$-statistic for all grid nodes is long. Then it is crucial to use in the computation the fast numerical algorithms. Because the computation of the $\mathcal{F}$-statistic involves calculation of the Fourier transform, one would like to use the *fast Fourier transform* (FFT) algorithm. As is known, the FFT algorithm computes the values of the *discrete Fourier transform* (DFT) of a time series for a certain set of discrete frequencies called the *Fourier frequencies*. Thus it will be possible to use the FFT algorithm in computation of the $\mathcal{F}$-statistic, provided the grid points will be arranged in such a way, that the frequency coordinates of these points will all coincide with the Fourier frequencies. We have constructed two different families of grids which fulfill this requirement. Our constructions were motivated by a simple observation (see Fig. 1) that the shape of the autocovariance ellipse strongly depends on the value of the parameter $\chi_{\rm i}$: the larger $|\chi_{\rm i}|$ is, the more alongated (along the frequency axis) this ellipse is. The usage of alongated ellipses suggests that the $\mathcal{F}$-statistic could be computed for smaller number of frequency values than the standard DFT algorithm computes. Therefore we have employed some modifications of the DFT algorithm leading to non-standard frequency resolutions achieved by zero padding or folding the data (this is discussed in Appendix A). Details of the grids construction are presented in Appendix B, where also the components of the basis vectors spanning the grids are given (in Tables III–V).

The construction of efficient banks of templates for gravitational-wave searches was recently discussed in Ref. [22] (see also [23–26]), where random template banks and relaxed lattice coverings were considered. As explained above we are interested in searches involving data streams so long, that the time performance of the search crucially depends on the ability of using the FFT algorithm. This enforces the above-mentioned constraint which is not fulfilled by the grids considered in Ref. [22]. Therefore our work can be considered as being complementary to the studies performed in Ref. [22]. The grid fulfilling the constraint was constructed in Sec. IV of Ref. [12] in the case of all-sky search for almost monochromatic gravitational waves. In the search considered in [12] the signal's parameter space is 4-dimensional and the polynomial phase model can not be employed. However,

in Sec. IV C of [12], as an example of application of general algorithm devised in [12] to construct constrained grids, the two-dimensional grid for searches of signals with polynomial phase is considered. This grid has thickness equal to ∼1.8, whereas grids constructed in the current paper have thicknesses of ∼1.2 (all grids found by us have covering thicknesses which are only 0.1%–16% larger than the thickness of the optimal two-dimensional hexagonal covering).

In Sec. IV of the current paper we present the results of numerical simulations we performed to study the quality of grids constructed in Appendix B. These results are contained in Table II. From our simulations it follows that when considering the efficiency of a grid it is not enough to worry only about the thickness of the covering related with the grid. We see from Table II that for lattices which have the same thickness of covering, but one of them has basis vectors which are orthogonal to each other, the time used to compute the $\mathcal{F}$-statistics is at least two times shorter than the corresponding time for the lattice with non-orthogonal basis vectors.

II. AUTOCOVARIANCE FUNCTION OF THE $\mathcal{F}$-STATISTIC

We assume that the noise n in the detector is an additive, stationary, Gaussian, and zero-mean continuous stochastic process. Then the logarithm of the likelihood function is given by

$$\ln\,\Lambda[x] = (x|h) - \frac{1}{2}\,(h|h), \tag{2.1}$$

where x denotes the data from the detector, h is the deterministic signal we are looking for in the data, and $(\cdot\,|\,\cdot)$ is the scalar product between waveforms defined by

$$(h_1|h_2) := 4\,\mathrm{Re}\int_0^\infty \frac{\tilde{h}_1(f)\,\tilde{h}_2^*(f)}{S_n(f)}\,\mathrm{d}f, \tag{2.2}$$

where $\tilde{}$ stands for the Fourier transform, * denotes complex conjugation, and S_n is the *one-sided spectral density* (defined for frequencies $0 \le f < +\infty$) of the detector's noise n.

We are interested in *almost monochromatic* signals, i.e. such signals for which the modulus of the Fourier transform is concentrated (for frequencies $f \ge 0$) around some 'central' frequency $f_\mathrm{c} > 0$ and S_n is a slowly changing function of f in the vicinity of the frequency f_c. If both waveforms h_1 and h_2 in Eq. (2.2) have Fourier transforms concentrated around the same frequency f_c, then we can replace $S_n(f)$ in the integrand of (2.2) by $S_n(f_\mathrm{c})$ and, after employing the Parseval's theorem, approximate the scalar product by

$$(h_1|h_2) \cong \frac{2}{S_n(f_\mathrm{c})}\int_{t_\mathrm{i}-T_\mathrm{o}/2}^{t_\mathrm{i}+T_\mathrm{o}/2} h_1(t)\,h_2(t)\,\mathrm{d}t = \frac{2\,T_\mathrm{o}}{S_n(f_\mathrm{c})}\langle h_1 h_2\rangle. \tag{2.3}$$

Here $\langle t_\mathrm{i}-T_\mathrm{o}/2;\, t_\mathrm{i}+T_\mathrm{o}/2\rangle$ denotes observational interval, so T_o is the length of observation time, and $t_\mathrm{i}-T_\mathrm{o}/2$ is the moment at which the observation begins. The time averaging operator $\langle\,\cdot\,\rangle$ is defined by

$$\langle h\rangle := \frac{1}{T_\mathrm{o}}\int_{t_\mathrm{i}-T_\mathrm{o}/2}^{t_\mathrm{i}+T_\mathrm{o}/2} h(t)\,\mathrm{d}t. \tag{2.4}$$

Using the formula (2.3) we can write the log likelihood ratio from Eq. (2.1) as

$$\ln\Lambda[x] \cong \frac{2\,T_\mathrm{o}}{S_n(f_\mathrm{c})}\Big(\langle x\,h\rangle - \frac{1}{2}\langle h^2\rangle\Big). \tag{2.5}$$

We restrict to almost monochromatic signals with frequency drift given by the linear-in-time relation,

$$f(t) = f_0 + \dot{f}_0\,t, \tag{2.6}$$

so f_0 and $\dot{f}_0$ is the frequency and the first derivative of the frequency with respect to time, respectively, both taken at the time $t = 0$. The instantaneous frequency is related to the phase Ψ of the signal by

$$f(t) = \frac{1}{2\pi}\frac{\mathrm{d}\,\Psi(t)}{\mathrm{d}\,t}. \tag{2.7}$$

Making use of Eqs. (2.6) and (2.7), we obtain the time dependence of the phase Ψ:

$$\Psi(t) = 2\pi\int_0^t f(t')\,\mathrm{d}\,t' + \Psi_0 = 2\pi\,\left(f_0\,t + \frac{1}{2}\,\dot{f}_0\,t^2\right) + \Psi_0, \tag{2.8}$$

where Ψ_0 is the value of the phase Ψ at the time $t = 0$. It is convenient to define the *dimensionless* parameters

$$\omega_0 := 2\pi\,f_0\,T_\mathrm{o}, \qquad \omega_1 := \pi\,\dot{f}_0\,T_\mathrm{o}^2. \tag{2.9}$$

Using these parameters we can write the phase Ψ in the form

$$\Psi(t;\Psi_0,\omega_0,\omega_1) = \Phi(t;\omega_0,\omega_1) + \Psi_0, \tag{2.10}$$

where

$$\Phi(t;\omega_0,\omega_1) = \omega_0\frac{t}{T_\mathrm{o}} + \omega_1\left(\frac{t}{T_\mathrm{o}}\right)^2. \tag{2.11}$$

We further assume that the gravitational-wave signal h we are looking for has a constant amplitude h_0, so it can be written in the form

$$h(t;h_0,\Psi_0,\omega_0,\omega_1) = h_0\,\sin\big(\Phi(t;\omega_0,\omega_1) + \Psi_0\big). \tag{2.12}$$

Let us collect the parameters of the phase Φ into a 2-dimensional vector $\boldsymbol{\xi}$,

$$\boldsymbol{\xi} := (\omega_0,\omega_1). \tag{2.13}$$

Then the gravitational-wave signal h, Eq. (2.12), we can shortly write as

$$h(t; h_0, \Psi_0, \boldsymbol{\xi}) = h_0 \sin\big(\Phi(t;\boldsymbol{\xi}) + \Psi_0\big). \tag{2.14}$$

It is easy to maximize the likelihood ratio (2.5) for the signal (2.14) with respect to the parameters h_0 and Ψ_0. To do this it is convenient to introduce the new parameters h_1 and h_2:

$$h_1 := h_0 \cos\Psi_0, \quad h_2 := h_0 \sin\Psi_0, \tag{2.15}$$

and rewrite the signal h in the form

$$h(t; h_1, h_2, \boldsymbol{\xi}) = h_1 \sin\Phi(t;\boldsymbol{\xi}) + h_2 \cos\Phi(t;\boldsymbol{\xi}). \tag{2.16}$$

Making use of Eq. (2.16) and the identities $2\sin\alpha\cos\alpha = \sin 2\alpha$, $\cos^2\alpha = \frac{1}{2}(1+\cos 2\alpha)$, $\sin^2\alpha = \frac{1}{2}(1-\cos 2\alpha)$ we can represent the time average $\langle h^2\rangle$ as

$$\langle h^2\rangle = \frac{1}{2}(h_1^2 + h_2^2) + h_1 h_2 \langle \sin 2\Phi\rangle + \frac{1}{2}(h_2^2 - h_1^2)\langle\cos 2\Phi\rangle. \tag{2.17}$$

For observation times longer than few hours and for almost monochromatic signals with frequency of the order of hundreds or thousands hertz, we can make approximation

$$\langle \sin 2\Phi\rangle \cong 0, \quad \langle\cos 2\Phi\rangle \cong 0. \tag{2.18}$$

Then Eq. (2.17) can be approximated by

$$\langle h^2\rangle \cong \frac{1}{2}\,(h_1^2 + h_2^2). \tag{2.19}$$

With the aid of the equality (2.19) it is easy to compute the optimal signal-to-noise ratio ρ for the signal (2.16):

$$\rho := \sqrt{(h|h)} \cong h_0 \sqrt{\frac{T_\mathrm{o}}{S_n(f_\mathrm{c})}}. \tag{2.20}$$

Substituting Eqs. (2.19) and (2.16) into Eq. (2.5), we get the following formula for the likelihood ratio:

$$\ln\Lambda(x; h_1, h_2, \boldsymbol{\xi}) \cong \frac{2\,T_\mathrm{o}}{S_n(f_\mathrm{c})}\left(h_1\,\langle x \sin\Phi(t;\boldsymbol{\xi})\rangle + h_2\,\langle x\,\cos\Phi(t;\boldsymbol{\xi})\rangle - \frac{1}{4}(h_1^2 + h_2^2)\right). \tag{2.21}$$

To maximize $\ln\Lambda$ with respect to the parameters h_1 and h_2 we solve equations

$$\frac{\partial \ln\Lambda}{\partial h_i} = 0, \quad i = 1, 2. \tag{2.22}$$

The unique solution to these equations reads

$$\hat{h}_1 = 2\langle x \sin\Phi\rangle, \quad \hat{h}_2 = 2\langle x\cos\Phi\rangle. \tag{2.23}$$

Replacing in Eq. (2.21) the parameters h_1 and h_2 by their estimators $\hat{h}_1$ and $\hat{h}_2$ [given by Eqs. (2.23)], we obtain the reduced likelihood ratio which we call the *$\mathcal{F}$-statistic*:

$$\mathcal{F}(x;\boldsymbol{\xi}) := \ln\Lambda(x;\hat{h}_1,\hat{h}_2,\boldsymbol{\xi}) \cong \frac{2\,T_\mathrm{o}}{S_n(f_\mathrm{c})}\left(\langle x\,\sin\Phi(t;\boldsymbol{\xi})\rangle^2 + \langle x\,\cos\Phi(t;\boldsymbol{\xi})\rangle^2\right). \tag{2.24}$$

It is rather easy to rewrite the $\mathcal{F}$-statistic in still another form,

$$\mathcal{F}(x;\boldsymbol{\xi}) \cong \frac{2}{S_n(f_\mathrm{c})T_\mathrm{o}}\left|\int_{t_\mathrm{i}-T_\mathrm{o}/2}^{t_\mathrm{i}+T_\mathrm{o}/2} x(t)\exp\left(-\mathrm{i}\omega_1\Big(\frac{t}{T_\mathrm{o}}\Big)^2\right)\exp\left(-\mathrm{i}\omega_0\frac{t}{T_\mathrm{o}}\right)\mathrm{d}t\right|^2. \tag{2.25}$$

Thus the $\mathcal{F}$-statistic, up to a constant multiplication factor, is the modulus squared of the Fourier transform of the product of the data stream $x(t)$ by the exponential factor $\exp\big(-\mathrm{i}\omega_1(t/T_\mathrm{o})^2\big)$ which depends on the spindown paramerer ω_1.

For the construction of the bank of templates it is crucial to study the expectation value of the $\mathcal{F}$-statistic (2.24) in the case when the data x contains some gravitational-wave signal h, i.e.

$$x(t) = n(t) + h(t;\boldsymbol{\theta}'), \tag{2.26}$$

where $\boldsymbol{\theta}' = (h_1', h_2', \boldsymbol{\xi}')$ collects the parameters of the gravitational-wave signal present in the data [see Eq. (2.16)]. Let us denote this expectation value by E_1 (the subscript '1' means here that the average is computed in the case when the data contains some gravitational-wave signal), so we have

$$\mathrm{E}_1\{\mathcal{F}(x;\boldsymbol{\xi})\} = \mathrm{E}\{\mathcal{F}(n(t) + h(t;\boldsymbol{\theta}');\boldsymbol{\xi})\}. \tag{2.27}$$

We want to obtain an approximate analytical formula for this quantity. Making use of the following approximations

$$\langle \sin[\Phi(t;\boldsymbol{\xi}) + \Phi(t;\boldsymbol{\xi}')]\rangle \cong 0,\ \langle \cos[\Phi(t;\boldsymbol{\xi}) + \Phi(t;\boldsymbol{\xi}')]\rangle \cong 0, \tag{2.28}$$

after some computation we obtain

$$\mathrm{E}_1\{\mathcal{F}(x;\boldsymbol{\xi})\} \cong 1 + \frac{1}{2}\,\rho^2 \left(\big\langle \sin\big[\Phi(t;\boldsymbol{\xi}) - \Phi(t;\boldsymbol{\xi}')\big]\big\rangle^2 + \big\langle \cos\big[\Phi(t;\boldsymbol{\xi}) - \Phi(t;\boldsymbol{\xi}')\big]\big\rangle^2 \right), \tag{2.29}$$

where ρ is the signal-to-noise ratio from Eq. (2.20). The right-hand side of the above equation can be rewritten in terms of the autocovariance function C_0 of the $\mathcal{F}$-statistic (computed in the case when the data contains only noise); it is defined as

$$C_0(\boldsymbol{\xi},\boldsymbol{\xi}') := \mathrm{E}\big\{[\mathcal{F}(n;\boldsymbol{\xi}) - m_0(\boldsymbol{\xi})][\mathcal{F}(n;\boldsymbol{\xi}') - m_0(\boldsymbol{\xi}')]\big\}, \tag{2.30}$$

where m_0 is the signal-free average of $\mathcal{F}$:

$$m_0(\boldsymbol{\xi}) := \mathrm{E}\{\mathcal{F}(n;\boldsymbol{\xi})\}. \tag{2.31}$$

In Sec. IV of Ref. [10] it was shown that the autocovariance function C_0 computed for the gravitational-wave signal of the form (2.16) can be approximated by

$$C_0(\boldsymbol{\xi},\boldsymbol{\xi}') \cong \big\langle \sin\big[\Phi(t;\boldsymbol{\xi}) - \Phi(t;\boldsymbol{\xi}')\big]\big\rangle^2 + \big\langle \cos\big[\Phi(t;\boldsymbol{\xi}) - \Phi(t;\boldsymbol{\xi}')\big]\big\rangle^2, \tag{2.32}$$

therefore the expectation value (2.29) can shortly be written as

$$\mathrm{E}_1\{\mathcal{F}(x;\boldsymbol{\xi})\} \cong 1 + \frac{1}{2}\,\rho^2\, C_0(\boldsymbol{\xi},\boldsymbol{\xi}'). \tag{2.33}$$

The phase Φ [see Eq. (2.11)] of the gravitational-wave signal (2.16) depends linearly on the parameters $\boldsymbol{\xi}$, therefore the autocovariance function (2.32) depends only on the differences between the parameters $\boldsymbol{\xi}$ and $\boldsymbol{\xi}'$:

$$C_0(\boldsymbol{\xi},\boldsymbol{\xi}') \cong \langle \sin\Phi(t;\boldsymbol{\xi}-\boldsymbol{\xi}')\rangle^2 + \langle \cos\Phi(t;\boldsymbol{\xi}-\boldsymbol{\xi}')\rangle^2. \tag{2.34}$$

If one introduces $\boldsymbol{\tau} := \boldsymbol{\xi} - \boldsymbol{\xi}'$, one can thus write

$$C_0(\boldsymbol{\tau}) \cong \langle \cos\Phi(t;\boldsymbol{\tau})\rangle^2 + \langle \sin\Phi(t;\boldsymbol{\tau})\rangle^2. \tag{2.35}$$

Let us note that the function C_0 attains its maximal value equal to 1 for $\boldsymbol{\tau} = \mathbf{0}$.

We will numerically compute the autocovariance function (2.35) in two ways. First, the right-hand side of Eq. (2.35) can be expressed (without any additional approximations) in terms of the Fresnel integrals:

$$C_\mathrm{e}(\boldsymbol{\tau},\chi_\mathrm{i}) = \frac{\pi}{2\,|\omega_1|}\left(\left[\mathrm{F_c}\left(\frac{\omega_0 + \omega_1\,(2\chi_\mathrm{i}+1)}{\sqrt{2\,\pi\,|\omega_1|}} \right) - \mathrm{F_c}\left(\frac{\omega_0 + \omega_1\,(2\chi_\mathrm{i}-1)}{\sqrt{2\,\pi\,|\omega_1|}} \right) \right]^2 + \left[\mathrm{F_s}\left(\frac{\omega_0 + \omega_1\,(2\chi_\mathrm{i}+1)}{\sqrt{2\,\pi\,|\omega_1|}} \right) - \mathrm{F_s}\left(\frac{\omega_0 + \omega_1\,(2\chi_\mathrm{i}-1)}{\sqrt{2\,\pi\,|\omega_1|}} \right) \right]^2 \right), \tag{2.36}$$

where we have introduced the dimensionless variable

$$\chi_\mathrm{i} := \frac{t_\mathrm{i}}{T_\mathrm{o}}. \tag{2.37}$$

The Fresnel integrals are defined as[1]

$$\mathrm{F_s}(x) := \int_0^x \sin\left(\frac{\pi\,z^2}{2}\right)\mathrm{d}z, \tag{2.38a}$$

$$\mathrm{F_c}(x) := \int_0^x \cos\left(\frac{\pi\,z^2}{2}\right)\mathrm{d}z. \tag{2.38b}$$

We can also compute the right-hand side of Eq. (2.35) in an approximate way. To do this we expand (2.35) in Taylor series around $\boldsymbol{\tau} = \mathbf{0}$ up to terms quadratic in $\boldsymbol{\tau}$. Making use of the obvious equalities

$$\Phi(t;\boldsymbol{\xi} = \mathbf{0}) = 0, \quad \frac{\partial^2\Phi}{\partial\xi_i\partial\xi_j} = 0, \tag{2.39}$$

[1] Let us note that both $\mathrm{F_c}$ and $\mathrm{F_s}$ are *odd* functions: $\mathrm{F_c}(-x) = -\mathrm{F_c}(x)$ and $\mathrm{F_s}(-x) = -\mathrm{F_s}(x)$.

we get

$$C_{\rm a}(\boldsymbol{\tau},\chi_{\rm i}) \cong 1 - \sum_{k,l=1}^{2} \tilde{\Gamma}(\chi_{\rm i})_{kl}\,\tau_k\,\tau_l, \tag{2.40}$$

where $\tilde{\Gamma}$ is the 2-dimensional *reduced Fisher information matrix* with elements equal to

$$\tilde{\Gamma}_{kl} := \Big\langle \frac{\partial\Phi}{\partial\tau_k}\frac{\partial\Phi}{\partial\tau_l}\Big\rangle - \Big\langle\frac{\partial\Phi}{\partial\tau_k}\Big\rangle\Big\langle\frac{\partial\Phi}{\partial\tau_l}\Big\rangle, \quad k,l=1,2. \tag{2.41}$$

In terms of the dimensionless variable $\chi_{\rm i}$ the Fisher matrix $\tilde{\Gamma}$ equals

$$\tilde{\Gamma}(\chi_{\rm i}) = \begin{pmatrix} \frac{1}{12} & \frac{1}{6}\,\chi_{\rm i} \\ \frac{1}{6}\,\chi_{\rm i} & \frac{1}{180} + \frac{1}{3}\,\chi_{\rm i}^2 \end{pmatrix}. \tag{2.42}$$

In Fig. 1 we study the relation between the exact (2.36) and approximate (2.40) formulae for the autocovariance function. We have found (see the left panel of Fig. 1) that the approximate formula underestimates the value of the autocovariance function. In the right panel of Fig. 1 we plot the isoheights of the approximate autocovariance function and the isoheights of the fractional difference

$$\Delta C := \frac{C_{\rm e} - C_{\rm a}}{C_{\rm e}} 100\%. \tag{2.43}$$

One can see that always $\Delta C > 0$ and for $C_{\rm e} \geq 0.75$ the fractional difference $\Delta C < 4\%$.

From Fig. 1 one can also see that whereas the isoheights of the approximate autocovariance $C_{\rm a}$ are perfect ellipses, the isoheights of the exact autocovariance $C_{\rm e}$ are closed curves of shapes very similar to that of ellipses. Therefore it is reasonable to study the value of the approximate autocovariance along the isoheight $C_{\rm e} = {\rm const}$ of the exact autocovariance. We have done this for the several values of $C_{\rm e}$. Along each $C_{\rm e} = {\rm const}$ curve the values of the approximate autocovariance are smaller than $C_{\rm e}$ and they are almost the same. We have picked up the largest value out of them and these values are given in Table I together with the corresponding values of $C_{\rm e}$ and the fractional difference between $C_{\rm a}$ and $C_{\rm e}$. The following cubic fit,

$$C_{\rm e} = -0.823872 + 3.15065\,C_{\rm a} - 1.84055\,C_{\rm a}^2 + 0.514037\,C_{\rm a}^3, \tag{2.44}$$

reproduces the relation $C_{\rm e} = C_{\rm e}(C_{\rm a})$ with accuracy better than 0.04% for $0.55 \leq C_{\rm a} \leq 1.00$.

TABLE I. The relation between the exact, Eq. (2.36), and the approximate, Eq. (2.40), formulae of the autocovariance function of the $\mathcal{F}$-statistic.

$C_{\rm e}$	$C_{\rm a}$	$(C_{\rm e} - C_{\rm a})/C_{\rm e}$
0.55	0.43767	20.4%
0.60	0.51513	14.2%
0.65	0.58769	9.6%
0.70	0.65600	6.3%
0.75	0.72057	3.9%
0.80	0.78183	2.3%
0.85	0.84012	1.2%
0.90	0.89575	0.5%
0.95	0.94897	0.1%

III. BANKS OF THE TEMPLATES

To search for the gravitational-wave signal (2.14) in detector's noise we need to construct a bank of templates in the space of the parameters (ω_0, ω_1) on which the $\mathcal{F}$-statistic [given in Eq. (2.24)] depends. The bank of templates is defined by a discrete set of points, i.e. a *grid* in the parameter space chosen in such a way, that for any possible signal there exists a grid point such that the expectation value of the $\mathcal{F}$-statistic computed for the parameters of this grid point is not less than a certain fixed minimal value. From Eq. (2.33) we see that this expectation value depends on the signal-to-noise ratio ρ and on the value of the noise autocovariance function C_0 computed for the intrinsic parameters $\boldsymbol{\xi}$ and $\boldsymbol{\xi}'$ of the template and the gravitational-wave signal, respectively. *In the rest of this paper we will approximate the autocovariance function C_0 by means of the formula* (2.40), i.e. we will use the equality $C_0(\boldsymbol{\xi},\boldsymbol{\xi}') \cong C_{\rm a}(\boldsymbol{\xi},\boldsymbol{\xi}')$.

The signal-to-noise ratio ρ we can not control, therefore to construct the bank of templates one needs to choose some minimum value $C_{\rm min}$ of the autocovariance function $C_{\rm a}$ and look for such a grid of points that for any point $\boldsymbol{\xi}'$ in the (ω_0, ω_1) plane there exists a grid node $\boldsymbol{\xi}$ such that the autocovariance $C_{\rm a}$ computed for the parameters $\boldsymbol{\xi}$ and $\boldsymbol{\xi}'$ is not less than $C_{\rm min}$. Because $C_{\rm a}$ depends on $\boldsymbol{\xi}$, $\boldsymbol{\xi}'$ only through the difference $\boldsymbol{\xi} - \boldsymbol{\xi}'$, we require that

$$C_{\rm a}(\boldsymbol{\xi} - \boldsymbol{\xi}') \geq C_{\rm min}. \tag{3.1}$$

By virtue of Eq. (2.40) this condition leads to the inequality

$$\sum_{k,l=1}^{2} \tilde{\Gamma}_{kl}\,(\xi_k - \xi'_k)\,(\xi_l - \xi'_l) \leq 1 - C_{\rm min}, \tag{3.2}$$

which for the fixed $\boldsymbol{\xi}$ is fulfilled by all points $\boldsymbol{\xi}'$ which belong to an ellipse with the center located at $\boldsymbol{\xi}$.

Wa want to find the *optimal* grid fulfilling the requirement (3.1), i.e. the grid which consists of possibly smallest number of points. Thus the problem of finding the optimal grid is a kind of *covering* problem, i.e. the problem to cover the (ω_0, ω_1) plane (or, in data analysis case, the bounded region of the plane) by the smallest number of *identical* ellipses. The thorough exposition of the problem of covering n-dimensional Euclidean space by identical spheres is given in Chap. 2 of Ref. [27].

We restrict ourselves to grids which are *lattices*, i.e. to grids with nodes which are linear combinations (with integer coefficients) of two basis vectors. If the vectors ($\mathbf{P}_0$, $\mathbf{P}_1$) are the basis vectors of a lattice, then a *fundamental*

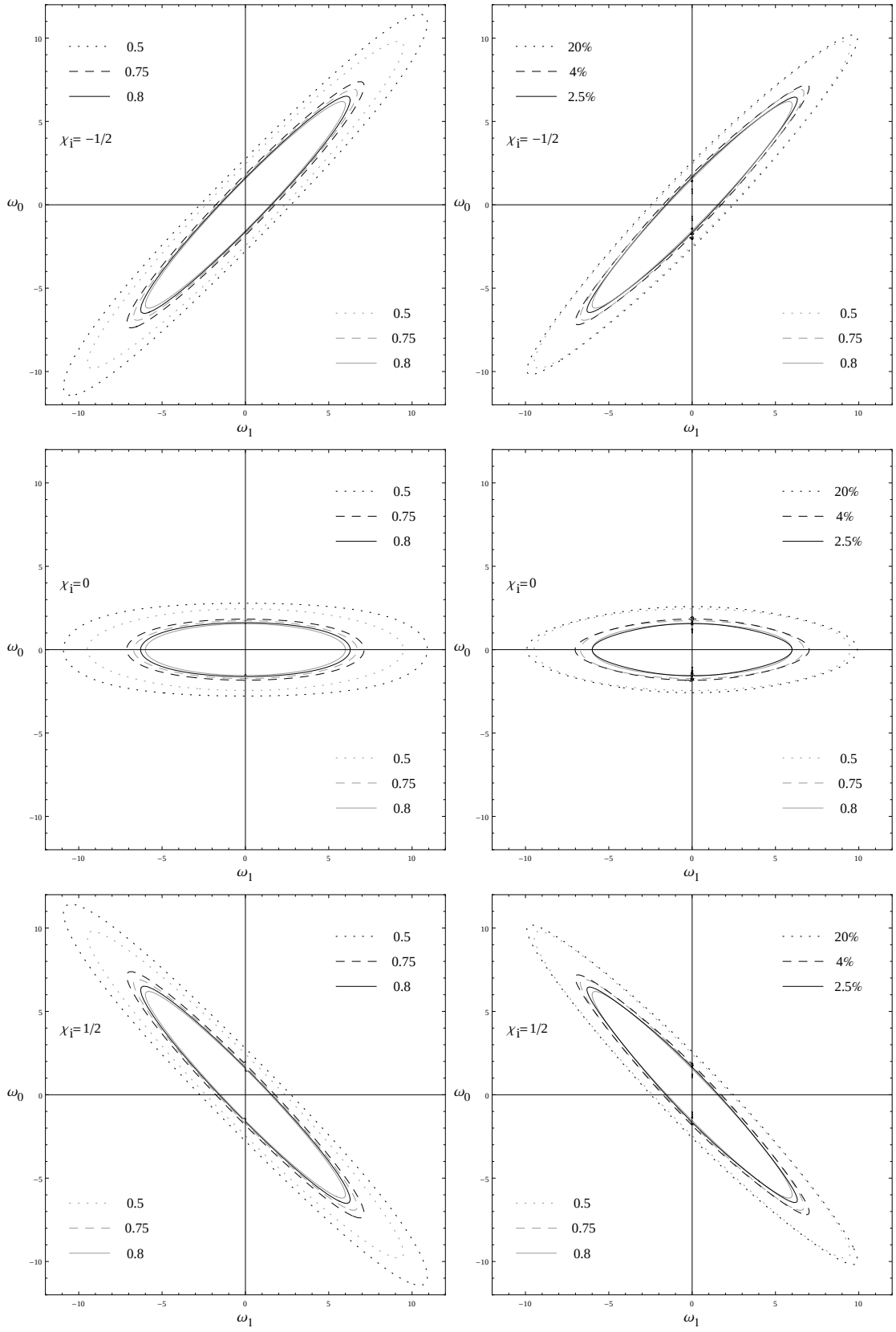

FIG. 1. Left panel: isoheights of the autocovariance function computed by means of the exact formula (2.36) (black lines) and the approximate formula (2.40) (grey lines); isoheights for the values 0.5, 0.75, and 0.8 are shown. Right panel: isoheights of the autocovariance function computed by means of the approximate formula (2.40) (grey lines) and isoheights of the fractional difference ΔC defined in Eq. (2.43) (black lines).

parallelogram (for the case of more than two parameters it would be a parallelotope) is the parallelogram consisting of the points

$$\lambda_0 \mathbf{P}_0 + \lambda_1 \mathbf{P}_1, \quad 0 \leq \lambda_0, \lambda_1 \leq 1. \tag{3.3}$$

A fundamental parallelogram is an example of a *fundamental region* for the lattice, which when repeated many times fills the plane with one lattice point in each copy. The quality of a covering can be expressed by the *covering thickness* θ which is defined as the average number of ellipses that contain a point in the plane. For lattice coverings their thickness can be computed as

$$\theta = \frac{\text{area of one ellipse}}{\text{area of fundamental region}}. \tag{3.4}$$

We assume that we are interested in such searches for almost monochromatic gravitational-wave signals for which the number of grid points in the parameter space is very large and the time needed to compute the $\mathcal{F}$-statistic for all grid nodes is long, so it is crucial to use in the computation the fast numerical algorithms. Because the computation of the $\mathcal{F}$-statistic involves calculation of the Fourier transform [see Eq. (2.25)], one would like to use the *fast Fourier transform* (FFT) algorithm. The FFT algorithm computes the values of the *discrete Fourier transform* (DFT) of a time series. The values of the DFT are defined for a certain set of discrete frequencies called the *Fourier frequencies*. It will thus be possible to use the FFT algorithm in computation of the $\mathcal{F}$-statistic, if the grid points will be arranged in such a way, that the frequency coordinates of these points will all coincide with the Fourier frequencies. We have constructed two different families of grids which fulfill this requirement, details of the construction are presented in Appendix B. In the construction we have explored observation that the shape of the autocovariance ellipse strongly depends on the value of the parameter χ_{i}: the larger $|\chi_{\mathrm{i}}|$ is, the more alongated (along the ω_0-axis) this ellipse is (see Fig. 1). But the usage of alongated enough ellipses suggests that the $\mathcal{F}$-statistic could be computed for smaller number of frequency values than the standard DFT algorithm computes. Therefore we have employed some modifications of the DFT algorithm.

Le the data collected by a detector form a sequence of N samples

$$x_u, \quad u = 1, \ldots, N, \tag{3.5}$$

and let the sampling period be Δt. Then the DFT algorithm calculates the Fourier transform of the data with the frequency resolution $\Delta f = 1/(N\Delta t)$. The resolution of the dimensionless frequency parameter ω_0 [introduced in Eq. (2.9)] is thus

$$\Delta\omega_0 = 2\pi T_{\mathrm{o}} \Delta f = 2\pi, \tag{3.6}$$

because $N\Delta t = T_{\mathrm{o}}$. It is possible to modify the DFT algorithm in such a way, that the frequency resolution (3.6) changes. In Appendix A we consider two such modifications: (i) zero-padding of the data, which makes the DFT more dense; (ii) folding of the data, which diminishes the frequency resolution. Therefore we study banks of templates which are compatible with the frequency resolutions of the form

$$\Delta\omega_0 = 2^\ell \pi, \quad \ell = 0, 1, 2, 3. \tag{3.7}$$

As explained in Appendix A, $\ell = 0$ corresponds to zero-padding of the data (for N data points we add N zeros), $\ell = 1$ is a pure DFT of N-point data stream, for $\ell = 2$ the data is folded two times and for $\ell = 3$ the data is folded four times.

Let $(\mathbf{P}_0, \mathbf{P}_1)$ be the basis vectors of a lattice we consider. As explained above we want to use the DFT algorithm, therefore we need a such bank of templates that all nodes can be arranged along straight lines parallel to the ω_0-axis. Moreover, the distance between neighboring nodes along these lines must be equal to the frequency resolution (3.7) of the DFT algorithm. To fulfill this constraint we require that the vector $\mathbf{P}_0$ has components

$$\mathbf{P}_0 = (\Delta\omega_0 = 2^\ell \pi,\, 0). \tag{3.8}$$

Let us also denote the components of the second basis vector $\mathbf{P}_1$ as

$$\mathbf{P}_1 = (\delta\omega_0, \delta\omega_1). \tag{3.9}$$

We will call the grid *orthogonal*, if $\mathbf{P}_0 \cdot \mathbf{P}_1 = 0$, where dot denotes the usual Euclidean scalar product. The grid spanned by the vectors (3.8) and (3.9) is thus orthogonal if and only if $\delta\omega_0 = 0$.

In Appendix B we have constructed two different families of grids fulfilling the constraint (3.8). Construction of the grids denoted by $\mathrm{G}_{1,\ell}$ (for $\ell = 0, 1, 2, 3$) is described in Appendix B 1, the grids $\mathrm{G}_{2,\ell}$ and $\mathrm{G}'_{2,\ell}$ (valid for $\ell = 1, 2, 3$) are constructed in Appendix B 2 a, and the grids $\mathrm{G}_{2,0}$ and $\mathrm{G}'_{2,0}$ are described in Appendix B 2 b. The grids $\mathrm{G}_{1,\ell}$ and $\mathrm{G}'_{2,\ell}$ are orthogonal, whereas the grids $\mathrm{G}_{2,\ell}$ are non-orthogonal.

IV. TIME PERFORMANCE OF THE GRIDS

We have made a number of numerical simulations to study the performance of the grids constructed in Appendix B. All computations were done for $N = 2^{19} = 524288$ data points. For the sampling period $\Delta t = 0.5$ s (i.e. for the Nyquist frequency equal to 1 Hz) this corresponds to around three days of data. The dimensionless first spindown parameter ω_1 we have taken to be non-positive and in the range $\omega_1 \in \langle -3000; 0 \rangle$. The discrete-in-time version of the $\mathcal{F}$-statistic [its continuous-in-time form is given in Eq. (2.25)] reads

$$\mathcal{F}(x;\boldsymbol{\xi}) \cong \frac{2\Delta t^2}{S_n(f_c)T_o}\left|\sum_{u=1}^{N} x_u \exp\left[-i\omega_1\left(\chi_i - \frac{1}{2} + \frac{u-1}{N}\right)^2\right]\exp\left(-i\omega_0\frac{u-1}{N}\right)\right|^2, \tag{4.1}$$

where the discrete data stream points are defined as $x_u := x\big(t_i - T_o/2 + (u-1)\Delta t\big)$ $(u = 1,\ldots,N)$. The DFT algorithm computes the sum present in Eq. (4.1) simultaneously for all dimensionless frequencies ω_0 from a discrete set. Let us denote these discrete Fourier frequencies by ω_{0r}, then (see Appendix A)

$$\omega_{0r} = (r-1)\,\Delta\omega_0, \quad r = 1,\ldots,r_{\max}, \tag{4.2}$$

where $\Delta\omega_0$ is the frequency resolution of the DFT. Using in the parameter space a discrete grid spanned by the vectors $(\mathbf{P}_0, \mathbf{P}_1)$ [see Eqs. (3.8) and (3.9)] means that also the spindown parameter ω_1 becomes discrete with possible values equal to

$$\omega_{1s} = -(s-1)\,\delta\omega_1, \quad s = 1,\ldots,s_{\max}. \tag{4.3}$$

In the case of non-orthogonal grids the point in the parameter space with coordinates $(\omega_0 = 0, \omega_{1s})$ usually is not a grid node for $s \neq 0$; the grid node with the smallest ω_0-coordinate is $(\mathrm{mod}(s\,\delta\omega_0, \Delta\omega_0), \omega_{1s})$, where $\mathrm{mod}(m,n)$ is the remainder on division of m by n. It means that for the fixed value of $s \neq 0$, before computing the DFT one has to multiply the uth data point by an extra exponential factor $\exp[-i\,\mathrm{mod}(s\,\delta\omega_0, \Delta\omega_0)u/N]$.

Collecting all this information together one can finally show that the $\mathcal{F}$-statistic evaluated on the grid point defined by the integers (r,s) [introduced in Eqs. (4.2) and (4.3)] can be written as

$$\mathcal{F}(x;r,s) \cong \frac{2\Delta t^2}{S_n(f_c)T_o}\left|\sum_{u=1}^{N} x_u \exp\left[i\,(s-1)\,\delta\omega_1\left(\chi_i - \frac{1}{2} + \frac{u-1}{N}\right)^2 - i\,\mathrm{mod}(s\,\delta\omega_0, \Delta\omega_0)\frac{u}{N}\right]\right.$$
$$\left.\times \exp\left[-i\,(r-1)\,\Delta\omega_0\frac{u-1}{N}\right]\right|^2, \quad r = 1,\ldots,r_{\max},\ s = 1,\ldots,s_{\max}. \tag{4.4}$$

In our numerical simulations we have used the FFT algorithm[2] with different frequency resolutions given in Eq. (3.7). In Table II we have shown the results of simulations in which we have studied, for different types of grids, the time needed to compute the $\mathcal{F}$-statistic for all grid nodes and the number of Fourier transforms performed during the computation.[3] We have also shown the thicknesses θ of coverings for different grids.

Let us remind that in two dimensions the optimal covering (without any constraint imposed) is the hexagonal covering with thickness θ equal to $2\pi/(3\sqrt{3}) \cong 1.2092$. The grids presented in Table II have all thicknesses in the range $1.2106 \lesssim \theta \lesssim 1.3990$, so they are greater than the optimal hexagonal covering thickness by $\sim$0.1% to $\sim$15.7%. From inspection of Table II it is clear that the value of the thickness does not decide on efficiency of a grid. We see that the most efficient grids are grids which involve the computation of the longest FFTs. Moreover, within the grids with the same value of ℓ (i.e. with the same length of the FFTs), much more efficient are orthogonal grids. The reason for this is the lack of the exponential term $\exp[-i\,\mathrm{mod}(s\,\delta\omega_0, \Delta\omega_0)u/N]$ in the discrete form of the $\mathcal{F}$-statistic, see Eq. (4.4).

The non-orthogonal grid $G''_{2,0}$ is identical to the grid $G_{2,0}$, but the time-performances of these two grids are different, because of different way of handling, during the computation of the $\mathcal{F}$-statistics, the exponential term $\exp[-i\,\mathrm{mod}(s\,\delta\omega_0, \Delta\omega_0)u/N]$ in Eq. (4.4). The computing time can be considerably reduced if the values of this term are computed in advance for all needed values of s and u and they are kept in RAM memory of computer (note that the exponential term depends on the quantities $\Delta\omega_0$ and $\delta\omega_0$ defining the grid and does not depend on data). However, to apply this trick one has to reserve a large amount of RAM for the table with values of the exponential term. For $\ell = 0$ (i.e. for the grid $G''_{2,0}$) this table requires about 2.5 GB of RAM. One can estimate that the table for $\ell + 1$ requires around 2 times more RAM than the table for ℓ.

[2] We have employed the fftw 3.2.2 implementation of the FFT algorithm with the wisdom mechanism (within which the algorithm performs some tests to ensure the optimal FFT performance).

[3] Our codes were written in C and compiled with gcc 4.3.4. We have used PC computer with Core 2 Quad 2.66 GHz processor and 4 GB of RAM.

TABLE II. The results of numerical simulations showing the time performance of the grids constructed in Appendix B. Besides the times needed to compute the $\mathcal{F}$-statistic [given in Eq. (4.4)] for all grid nodes, the number of the FFTs calculated during the computation and the covering thicknesses θ are also shown. All grids are constructed for $C_{\min} = 0.75$ (which corresponds to $C^{\mathrm{e}}_{\min} = 0.7737$). Each time slot in the table is the arithmetic mean from 200 repetitions of the computation of the $\mathcal{F}$-statistic for all grid nodes.

	$\mathrm{G}_{1,\ell}$			$\mathrm{G}_{2,\ell}$, $\mathrm{G}'_{2,\ell}$, $\mathrm{G}''_{2,\ell}$				
				Time (s)				
ℓ	Time (s)	No of FFTs	θ	$\mathrm{G}_{2,\ell}$	$\mathrm{G}'_{2,\ell}$	$\mathrm{G}''_{2,\ell}$	No of FFTs	θ
0	23.4	318	1.2287	48.1	23.1	30.4	315	1.2186
1	31.3	705	1.3639	81.7	32.2	–	723	1.3990
2	38.2	1273	1.2325	126.6	38.8	–	1276	1.2351
3	63.0	2676	1.2954	230.2	59.1	–	2501	1.2106

Appendix A: Modifications of the discrete Fourier transform

The data from the detector form the sequence

$$(x_r) = (x_1, x_2, \ldots, x_N), \tag{A1}$$

so N is the number of data points. The discrete Fourier transform (DFT) of the data (A1) is defined as

$$\tilde{x}_s = \sum_{r=1}^{N} x_r \exp\left(-2\pi \mathrm{i} \frac{(r-1)(s-1)}{N} \right), \quad s = 1, \ldots, N. \tag{A2}$$

The DFT defined above computes the Fourier transform of the data stream (A1) at frequencies

$$f_s = \frac{s-1}{N\Delta t} = 2(s-1)\frac{f_{\mathrm{N}}}{N}, \quad s = 1, \ldots, N, \tag{A3}$$

where Δt is the sampling period and f_{N} is the Nyquist frequency. The frequency resolution of the DFT (A2) is thus

$$\Delta f = \frac{1}{N\Delta t} \implies \Delta\omega_0 = 2\pi. \tag{A4}$$

1. Zero padding

Let us now consider the $2N$-point data stream (y_r) which consists of the original N-point data stream (x_r), Eq. (A1), supplemented by N zeros,

$$(y_r) = (x_1, \ldots, x_N, 0, \ldots, 0). \tag{A5}$$

By virtue of formula (A2), the DFT of the data (y_r) reads

$$\tilde{y}_s = \sum_{r=1}^{N} x_r \exp\left(-2\pi \mathrm{i} \frac{(r-1)(s-1)}{2N} \right), \quad s = 1, \ldots, 2N. \tag{A6}$$

Making use of Eqs. (A2) and (A3) one easily sees, that the numbers $\tilde{y}_s$ can be interpreted as the values of the DFT of the original data stream (x_r), but computed now for frequences

$$f_s = \frac{s-1}{2N\Delta t}, \quad s = 1, \ldots, 2N, \tag{A7}$$

so the frequency resolution of the DFT (A6) is

$$\Delta f = \frac{1}{2N\Delta t} \implies \Delta\omega_0 = \pi. \tag{A8}$$

Of course one can add more zeros to the data to obtain their DFT with the frequency resolution better than this given in Eq. (A8).

2. Folding of data

Let us fold the N-point data stream (x_r) to the $(N/2)$-point data stream (y_r),

$$y_r := x_r + x_{r+N/2}, \quad r = 1, \ldots, \frac{N}{2}. \tag{A9}$$

The DFT of the data (y_r) reads, according to Eq. (A2),

$$\tilde{y}_s = \sum_{r=1}^{N/2} (x_r + x_{r+N/2}) \exp\left(-2\pi \mathrm{i} \frac{(r-1)(s-1)}{N/2} \right), \quad s = 1, \ldots, \frac{N}{2}. \tag{A10}$$

It is not difficult, employing the periodicity of the function $\exp(\mathrm{i}z)$ for real z, to rewrite formula (A10) in the form

$$\tilde{y}_s = \sum_{r=1}^{N} x_r \exp\left(-2\pi \mathrm{i} \frac{2(r-1)(s-1)}{N} \right), \quad s = 1, \ldots, \frac{N}{2}. \tag{A11}$$

Again making use of Eqs. (A2) and (A3) one sees, that the numbers $\tilde{y}_s$ can be interpreted as the values of the DFT of the original data stream (x_r), but computed for frequences

$$f_s = \frac{2(s-1)}{N\Delta t}, \quad s = 1, \ldots, \frac{N}{2}, \tag{A12}$$

so the frequency resolution of the DFT (A11) is

$$\Delta f = \frac{2}{N\Delta t} \implies \Delta\omega_0 = 4\pi. \tag{A13}$$

By folding the data p times ($p = 1, 2, \ldots$) one gets (N/p)-point data stream the DFT of which is the DFT of the original N-point data but computed with the frequency resolution $\Delta\omega_0 = 2^p \times 2\pi$.

Appendix B: Construction of the grids in the parameter space

1. Grids G_1

In this appendix we construct a family of grids by construction of their fundamental regions of parallelogram shape. The fundamental parallelograms are always inscribed into the ellipse of constant value of the autocovariance function [this ellipse is given by Eq. (3.2)] and their construction ensures that the constraint (3.7) is fulfilled.

a. Construction of the fundamental parallelogram

Let us denote the coordinates of the parallelogram vertexes we are looking for by $(\omega_0^{(a)}, \omega_1^{(a)})$, $a = 1, \ldots, 4$. Bases of the parallelogram we choose to be parallel to the ω_1 axis, so the ω_0 coordinates of the vertexes can be written as

$$\omega_0^{(a)}(k) = k\,\frac{\pi}{2}, \quad a = 1, 2, \quad \omega_0^{(a)}(k) = -k\,\frac{\pi}{2}, \quad a = 3, 4, \tag{B1}$$

where $k > 0$. Then the coordinates $\omega_1^{(a)}$ of the vertexes we obtain from the equations [here T denotes the transposition of the row vector $(\omega_0^{(a)}, \omega_1^{(a)})$]:

$$(\omega_0^{(a)}, \omega_1^{(a)}) \cdot \tilde{\Gamma}(\chi_\mathrm{i}) \cdot (\omega_0^{(a)}, \omega_1^{(a)})^\mathsf{T} = 1 - C^\mathrm{i}_\mathrm{min}, \quad a = 1, \ldots, 4, \tag{B2}$$

where $\tilde{\Gamma}(\chi_\mathrm{i})$ is the Fisher matrix from Eq. (2.42) and $C^\mathrm{i}_\mathrm{min}$ (the reason for introducing the extra subscript 'i', from 'initial', is explained in Appendix B 1 b below) is the minimum value of the autocovariance function. We can assume that $C^\mathrm{i}_\mathrm{min} \in (0;\, 1)$, then the solution of Eqs. (B2) reads

$$\omega_1^{(1)}(\chi_\mathrm{i}, k) = \frac{-30\,k\,\pi\,\chi_\mathrm{i} + \sqrt{15}\sqrt{48\,(1 - C^\mathrm{i}_\mathrm{min})\,(1 + 60\,\chi_\mathrm{i}^2) - k^2\,\pi^2}}{2\,(1 + 60\,\chi_\mathrm{i}^2)}, \tag{B3a}$$

$$\omega_1^{(2)}(\chi_\mathrm{i}, k) = \frac{-30\,k\,\pi\,\chi_\mathrm{i} - \sqrt{15}\sqrt{48\,(1 - C^\mathrm{i}_\mathrm{min})\,(1 + 60\,\chi_\mathrm{i}^2) - k^2\,\pi^2}}{2\,(1 + 60\,\chi_\mathrm{i}^2)}, \tag{B3b}$$

$$\omega_1^{(3)}(\chi_\mathrm{i}, k) = -\omega_1^{(2)}(\chi_\mathrm{i}, k), \qquad \omega_1^{(4)}(\chi_\mathrm{i}, k) = -\omega_1^{(1)}(\chi_\mathrm{i}, k). \tag{B3c}$$

Area of the parallelogram with the vertexes given above is equal to

$$S = (\omega_1^{(1)} - \omega_1^{(2)})\,k\,\pi. \tag{B4}$$

Making use of Eqs. (B3) we get the area S as a function of the parameters χ_i and k:

$$S(\chi_\mathrm{i}, k) = \frac{\sqrt{15}\sqrt{48\,(1 - C^\mathrm{i}_\mathrm{min})\,(1 + 60\,\chi_\mathrm{i}^2) - k^2\,\pi^2}}{1 + 60\,\chi_\mathrm{i}^2}\,k\,\pi. \tag{B5}$$

We want to have the fundamental parallelogram of possibly large area. Let us first fix the parameter χ_i and maximize the area with respect to the parameter k. The only positive solution of the equation $\partial S/\partial k = 0$ reads

$$k_0(\chi_\mathrm{i}) = \frac{2}{\pi}\,\sqrt{6\,(1 - C^\mathrm{i}_\mathrm{min})(1 + 60\,\chi_\mathrm{i}^2)}. \tag{B6}$$

We can compute the area of the parallelogram for this optimal value of k:

$$S_\mathrm{max} = S\big(\chi_\mathrm{i}, k_0(\chi_\mathrm{i})\big) = 24\sqrt{15}\,(1 - C^\mathrm{i}_\mathrm{min}). \tag{B7}$$

It does not depend on the vaule of χ_i. It can be shown that the value S_max given above is also the *global* maximum of the function $S = S(\chi_\mathrm{i}, k)$.

The dependence $S = S(\chi_\mathrm{i}, k)$ is illustrated in Fig. 2. It is easy to show that for any value of $k > k_\mathrm{min}$, where

$$k_\mathrm{min} := \frac{2}{\pi}\sqrt{6\,(1 - C^\mathrm{i}_\mathrm{min})}, \tag{B8}$$

we can find two values of χ_i for which the maximal area S_max is achieved. These values one obtains solving the equation $S(\chi_\mathrm{i}, k) = S_\mathrm{max}$. The solutions read

$$\chi_\mathrm{i}(k) = \pm\frac{\sqrt{k^2\,\pi^2 - 24(1 - C^\mathrm{i}_\mathrm{min})}}{12\sqrt{10\,(1 - C^\mathrm{i}_\mathrm{min})}}. \tag{B9}$$

For $k = k_\mathrm{min}$ we get only one solution $\chi_\mathrm{i}(k_\mathrm{min}) = 0$.

b. Construction of the grids

We want to use the FFT algorithm in the computation of the $\mathcal{F}$-statistic for all grid nodes, therefore we need such a grid that (i) all grid points can be arranged along straight lines parallel to the ω_0-axis, and (ii) the distance between neigbouring points along these lines is $k\pi$, where $k = 2^\ell$, $\ell = 0, 1, 2, 3$ [see Eq. (3.7)]. It is not difficult to construct an *orthogonal* lattice fulfilling

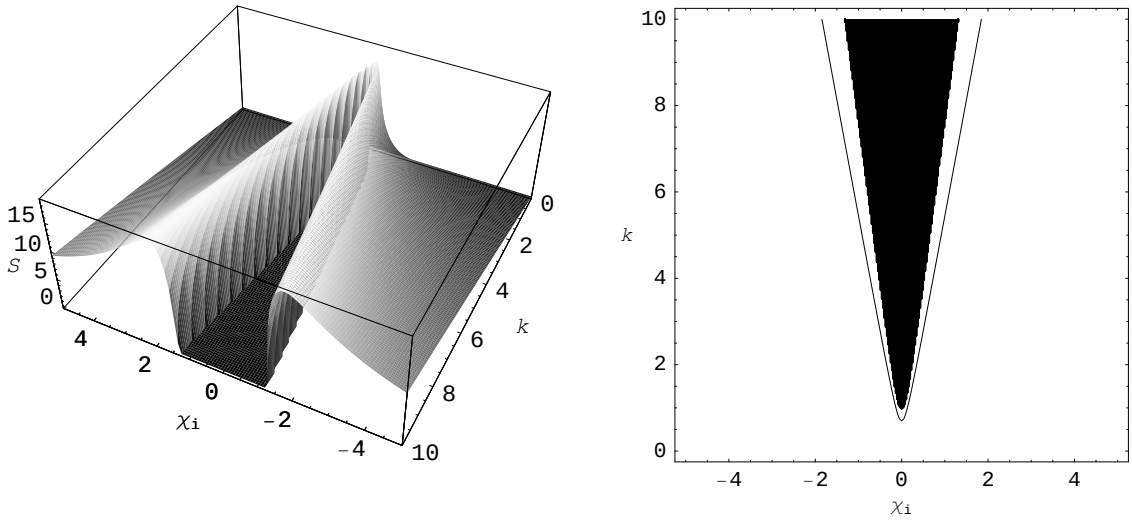

FIG. 2. In the left panel the area S of the fundamental parallelogram for the grid G_1 is plotted as a function of the parameters $\chi_{\rm i}$ and k [see Eq. (B5)]. In the right panel the part of the $(\chi_{\rm i}, k)$ plane is displayed; here the shaded region is made of the points $(\chi_{\rm i}, k)$ for which the construction of the parallelogram is not possible, and the V-shaped solid line is made of these values of the parameters $(\chi_{\rm i}, k)$ for which the maximal area $S_{\max}$ is achieved.

these requirements. Let the lattice be spanned by the vectors $(\mathbf{P}_0, \mathbf{P}_1)$. The first basis vector $\mathbf{P}_0$ is parallel to the ω_0-axis and has components $\mathbf{P}_0 := (k\pi, 0)$, so its length is equal to the height of the fundamental parallelogram. The second basis vector $\mathbf{P}_1$ is chosen to be parallel to the ω_1-axis and has length equal to the length of the parallelogram's base. The ω_1-component of the vector $\mathbf{P}_1$ can easily be obtained from Eqs. (B3). One finds that $\mathbf{P}_1 = (0, \delta\omega_1)$, where

$$\delta\omega_1 = \frac{\sqrt{15}\sqrt{48\,(1 - C^{\rm i}_{\rm min})\,(1 + 60\chi_{\rm i}^2) - k^2\,\pi^2}}{1 + 60\chi_{\rm i}^2}. \quad \text{(B10)}$$

In the construction of the fundamental parallelogram presented above (in Appendix B 1 a) we have ensured that the autocovariance between the center of the fundamental parallelogram and any of its vertexes is equal to $C^{\rm i}_{\rm min}$. In the bank of templates spanned by the vectors $\mathbf{P}_0$ and $\mathbf{P}_1$ the minimum value [taken over all points in the (ω_0, ω_1)-plane] of the maximum (taken over all grid points) autocovariance between any point in the (ω_0, ω_1)-plane and all the grid points is not less than $C^{\rm i}_{\rm min}$. It turns out that usually it is *greater* than $C^{\rm i}_{\rm min}$. Let us denote this minimum value of the autocovariance by $C_{\rm min}$, then $C_{\rm min} \geqslant C^{\rm i}_{\rm min}$.

To find the value of $C_{\rm min}$ we should first find the *Voronoi cell* of the grid.[4] To do this let us first choose

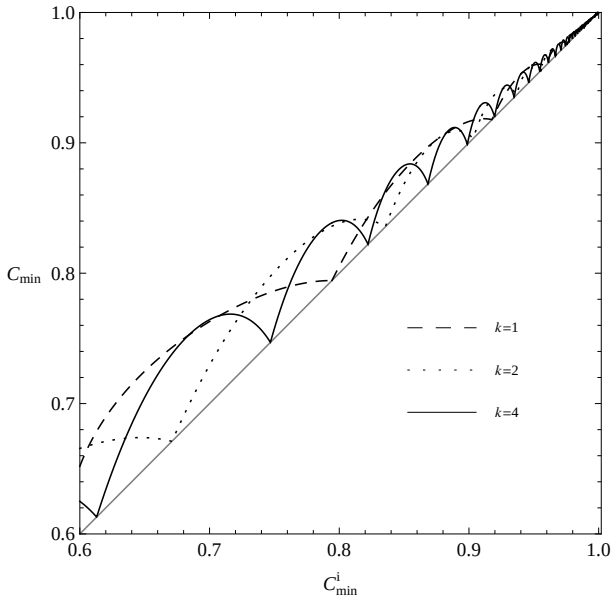

FIG. 3. The relation, valid for the grids G_1, between the initial minimum value $C^{\rm i}_{\rm min}$ and the final minimum value $C_{\rm min}$ of the autocovariance. Plots for three different values of the parameter k are shown. The diagonal grey line is the plot of the relation $C_{\rm min} = C^{\rm i}_{\rm min}$.

two neighbouring grid nodes and find all points in the (ω_0, ω_1)-plane such that the autocovariance between the point and one of the chosen nodes is equal to the autocovariance between the point and the second node. All

[4] With each point $\boldsymbol{\xi}_a$ of a lattice $\mathcal{L}$ we associate its *Voronoi cell* $\mathrm{V}(\boldsymbol{\xi}_a)$ which consists of those points of plane that are at least as close to $\boldsymbol{\xi}_a$ as to any other point $\boldsymbol{\xi}_b \in \mathcal{L}$: $\mathrm{V}(\boldsymbol{\xi}_a) := \{\boldsymbol{\zeta} : |\boldsymbol{\zeta} - \boldsymbol{\xi}_a| \leq |\boldsymbol{\zeta} - \boldsymbol{\xi}_b| \text{ for all } b\}$.

such points belong to the border between neighbouring Voronoi cells. We repeat this construction for all nodes which are neighbours of the chosen node. Points where borders cross each other are vertexes of the Voronoi cell and at these vertexes the autocovariance takes its minimum value. In Fig. 3 we have shown, for different values of the parameter k, the relation between the initial minimum value $C^{\rm i}_{\rm min}$ and the final minimum value $C_{\rm min}$ of the autocovariance.

2. Grids G_2

Constructions of the grids G_2 were inspired by the existence of the *optimal hexagonal covering* by circles of the 2-dimensional Cartesian space $\mathbb{R}^2$ and they can be treated as some deformations of this covering. To employ the properties of the hexagonal covering we firstly translate, by means of a linear transformation, the problem of covering the (ω_0,ω_1)-plane by identical *ellipses* to the problem of covering the (ω'_0,ω'_1)-plane by *unit circles*.

In the constructions of the grids described below we were guided by the two following features of the hexagonal covering. (i) The fundamental region of the hexagonal covering can be chosen to be a regular hexagon inscribed into the circle; we demand that deformed coverings have fundamental region in the form of a polygon (usually nonregular hexagon) inscribed into the unit circle. (ii) Let us denote by $(\mathbf{P}'_0,\mathbf{P}'_1)$ the basis vectors of the lattice covering in the (ω'_0,ω'_1)-plane (with the vector $\mathbf{P}'_0$ is parallel to the ω'_0-axis); we demand that the lattice points which lie along two neighbouring straight lines parallel to the vector $\mathbf{P}'_1$ are shifted with respect to each other by half of length of the vector $\mathbf{P}'_1$ (this feature can be seen in Fig. 4).

We start from constructing a linear transformation (described by a matrix M) which converts the ellipse of the autocovariance function into the circle of unit radius. The matrix M transforms a point with coordinates (ω_0,ω_1) into the point with coordinates (ω'_0,ω'_1):

$$(\omega'_0,\omega'_1)^{\mathsf{T}} = \mathsf{M}\cdot(\omega_0,\omega_1)^{\mathsf{T}}. \tag{B11}$$

Equation of the ellipse of the autocovariance function in the (ω_0,ω_1)-plane reads [see Eq. (B2)]

$$(\omega_0,\omega_1)\cdot\tilde{\Gamma}\cdot(\omega_0,\omega_1)^{\mathsf{T}} = 1 - C_{\rm min}. \tag{B12}$$

The linear transformation (B11) converts the ellipse (B12) into the circle of unit radius provided the matrix M fulfills the condition

$$\mathsf{M}^{\mathsf{T}}\cdot\mathsf{M} = \frac{1}{1-C_{\rm min}}\tilde{\Gamma}. \tag{B13}$$

The Fisher matrix $\tilde{\Gamma}$ is symmetric and [what can easily be shown by means of Eq. (2.42)] it is strictly positive definite, i.e. $(\omega_0,\omega_1)\cdot\tilde{\Gamma}\cdot(\omega_0,\omega_1)^{\mathsf{T}} > 0$ for any $(\omega_0,\omega_1)\neq(0,0)$. For such matrix $\tilde{\Gamma}$ the equation (B13) can be interpreted as its Cholesky decomposition, which states that there exists the unique upperdiagonal matrix M fulfilling Eq. (B13). In the rest of this subsection we will assume that the matrix M is the result of the Cholesky decomposition (so it is an upperdiagonal matrix). Let us also note that the matrix M depends on the parameters $\chi_{\rm i}$ and $C_{\rm min}$.

Let $\mathbf{P}_0$ be the vector in the (ω_0,ω_1)-plane parallel to the ω_0 axis and with length equal to $k\pi$, so its (ω_0,ω_1)-components are $\mathbf{P}_0 = (k\pi,0)$. After transformation to the (ω'_0,ω'_1)-plane this vector becomes $\mathbf{P}'_0$. Let us denote its length by $ak\pi$, thus its (ω'_0,ω'_1)-components are (remember that the matrix M is upperdiagonal)

$$\mathbf{P}'_0 = (ak\pi,0). \tag{B14}$$

The construction of the second basis vector $\mathbf{P}'_1$ of the lattice in the (ω'_0,ω'_1)-plane is described in details below. When this vector is found, we take its image in the transformation inverse to that from Eq. (B11), it defines the second basis vector in the (ω_0,ω_1)-plane,

$$\mathbf{P}_1 := \mathsf{M}^{-1}\mathbf{P}'_1. \tag{B15}$$

For the lattices constructed below the components of the basis vectors $\mathbf{P}_1$ depend on the parameter $\chi_{\rm i}$, therefore for different values of this parameter we get different lattices, but, as we checked, all these lattices have (for the fixed ℓ) the same value of covering thickness. Moreover, we can always choose such value of $\chi_{\rm i}$ that the vectors $\mathbf{P}_0$ and $\mathbf{P}_1$ will be orthogonal. In Table IV we give the components of the basis vectors $(\mathbf{P}_0,\mathbf{P}_1)$ for non-orthogonal grids $G_{2,\ell}$ (for $\ell=0,1,2,3$) defined by choosing $\chi_{\rm i}=0$. Table V contains the components of the vectors $(\mathbf{P}_0,\mathbf{P}_1)$ for orthogonal grids $G'_{2,\ell}$ (for $\ell=0,1,2,3$; we have added here primes to the grid symbols to distinguish them from non-orthogonal grids of Table IV) together with the values of the parameter $\chi_{\rm i}$ chosen to make the basis vectors orthogonal.

a. *Grids $G_{2,\ell}$ (valid for $\ell\geq 1$)*

To find the second basis vector $\mathbf{P}'_1$ in the (ω'_0,ω'_1)-plane, we make the following construction, which is illustrated in Fig. 4. We plot a circle K with radius equal to half of the length of the vector $\mathbf{P}'_0$. The center of the circle coincides with the center of the line segment spanned by the vector $\mathbf{P}'_0$. We inscribe a right-angled triangle G into the circle K, its hypotenuse is along the diameter of the circle (i.e. along the vector $\mathbf{P}'_0$). The vertex O at the right angle of the triangle G has coordinates

$$O = \left(\frac{1}{2}ak\pi - \sqrt{\frac{1}{4}(ak\pi)^2 - {\omega'_1}^2},\omega'_1\right). \tag{B16}$$

The second basis vector $\mathbf{P}'_1$ is chosen to be parallel to one of the sides of the triangle G, see Fig. 4. We demand that the ratio of the length L of this side and half of length

TABLE III. Basis vectors $\mathbf{P}_0$ and $\mathbf{P}_1$ defining the orthogonal grids $G_{1,\ell}$ ($\ell = 0, 1, 2, 3$) for $C_{\min} = 0.75$ (which corresponds to $C^{\rm e}_{\min} = 0.7737$). The covering thicknesses θ of the grids $G_{1,\ell}$ are shown in Table II.

ℓ	$C^{\rm i}_{\min}$	$\chi_{\rm i}$	$\mathbf{P}_0$	$\mathbf{P}_1$
0	0.68038480461	0.06911969777	$(\pi, 0)$	$(0, 9.4565868877)$
1	0.71208037943	0.28027281768	$(2\pi, 0)$	$(0, 4.2593984076)$
2	0.68138053992	0.57228732748	$(4\pi, 0)$	$(0, 2.3567814138)$
3	0.69684651733	1.19594612580	$(8\pi, 0)$	$(0, 1.1211909237)$

TABLE IV. Basis vectors $\mathbf{P}_0$ and $\mathbf{P}_1$ defining the non-orthogonal grids $G_{2,\ell}$ ($\ell = 0, 1, 2, 3$) for $C_{\min} = 0.75$ (which corresponds to $C^{\rm e}_{\min} = 0.7737$). The grids are defined by choosing $\chi_{\rm i} = 0$. The covering thicknesses θ of the grids $G_{2,\ell}$ are shown in Table II.

ℓ	$\chi_{\rm i}$	$\mathbf{P}_0$	$\mathbf{P}_1$
0	0	$(\pi, 0)$	(1.57079632679490, 9.53468292515346)
1	0	$(2\pi, 0)$	(1.91202057746303, 4.15260608129565)
2	0	$(4\pi, 0)$	(2.65356333373361, 2.35185575858832)
3	0	$(8\pi, 0)$	(2.92397504375649, 1.19974457106559)

TABLE V. Basis vectors $\mathbf{P}_0$ and $\mathbf{P}_1$ defining the orthogonal grids $G'_{2,\ell}$ ($\ell = 0, 1, 2, 3$) for $C_{\min} = 0.75$ (which corresponds to $C^{\rm e}_{\min} = 0.7737$). The values of the parameter $\chi_{\rm i}$ chosen to make the basis vectors orthogonal are also given. The covering thicknesses θ of the grids $G'_{2,\ell}$ are shown in Table II.

ℓ	$\chi_{\rm i}$	$\mathbf{P}_0$	$\mathbf{P}_1$
0	0.08237276158660	$(\pi, 0)$	(0, 9.53468292515345)
1	0.23021935382642	$(2\pi, 0)$	(0, 4.15260608129565)
2	0.56414244879677	$(4\pi, 0)$	(0, 2.35185575858833)
3	1.21858231921793	$(8\pi, 0)$	(0, 1.19974457106559)

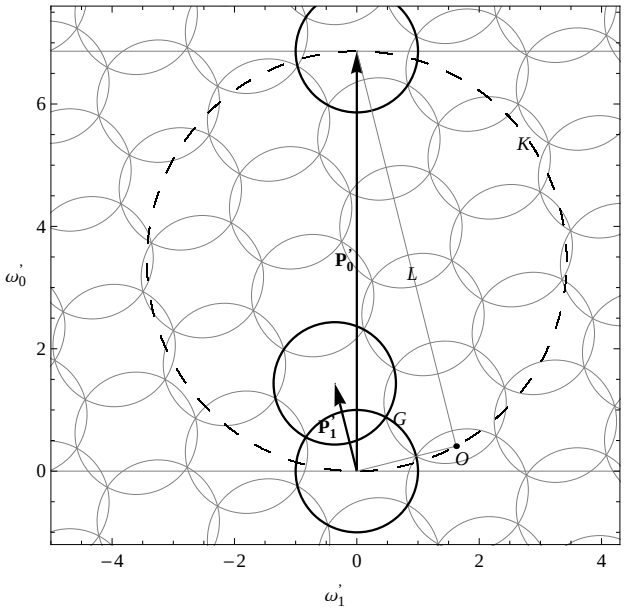

FIG. 4. Construction of the grids $G_{2,\ell}$ (valid for $\ell \geq 1$) in the (ω'_0, ω'_1)-plane.

of the vector $\mathbf{P}'_1$ is an odd positive integer, $L/(|\mathbf{P}'_1|/2) = 2n + 1$ ($n = 1, 2, \ldots$). For the fixed n this requirement fixes the both coordinates of the point O and thus it determines the vector $\mathbf{P}'_1$ uniquely. Usually we obtain several possible values of n. We choose this value which leads to lattice with the smallest covering thickness θ.

b. Grid $G_{2,0}$ (valid for $\ell = 0$)

The construction of the grid $G_{2,0}$ in the (ω'_0, ω'_1)-plane is illustrated in Fig. 5. We start from constructing three circles of unit radii. All these circles have to cross each other at the same point. We build then the three vectors $\mathbf{v}_1$, $\mathbf{v}_2$, and $\mathbf{v}_3$ of unit length ($|\mathbf{v}_1| = |\mathbf{v}_2| = |\mathbf{v}_3| = 1$). The vector $\mathbf{v}_1$ begins at the centre of one of the circles and ends at the point which is common to all three circles; the vectors $\mathbf{v}_2$ and $\mathbf{v}_3$ are constructed in a similar way, see Fig. 5. The coordinates of the vectors $\mathbf{v}_1$, $\mathbf{v}_2$, and $\mathbf{v}_3$ are

$$\mathbf{v}_1 = (p, q), \quad \mathbf{v}_2 = (p, -q), \quad \mathbf{v}_3 = (0, 1), \tag{B17}$$

where p and q are positive numbers fulfilling the condition

$$p^2 + q^2 = 1. \tag{B18}$$

Because (see Fig. 5)

$$\mathbf{P}'_0 = \mathbf{v}_1 + \mathbf{v}_2, \tag{B19}$$

by virtue of Eq. (B14) (taken for $k = 1$) we get

$$p = \frac{1}{2} a\pi. \tag{B20}$$

Making use of Eqs. (B18), (B20) and the equality (see Fig. 5)

$$\mathbf{P}'_1 = \mathbf{v}_1 + \mathbf{v}_3, \tag{B21}$$

one easily obtains the (ω'_0, ω'_1)-coordinates of the basis vector $\mathbf{P}'_1$,

$$\mathbf{P}'_1 = \left(\frac{1}{2}\pi a, 1 + \sqrt{1 - \left(\frac{1}{2}\pi a\right)^2} \right). \tag{B22}$$

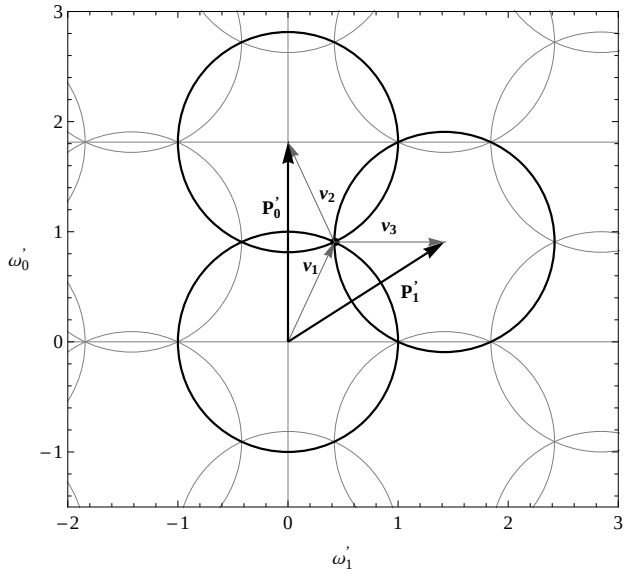

FIG. 5. Construction of the grid $G_{2,0}$ in the (ω_0', ω_1')-plane.

ACKNOWLEDGMENTS

The work presented in this paper was supported in part by the Polish MNiSzW grant no. N N203 387237. We would like to thank Andrzej Królak for helpful discussions.

[1] D. Sigg and the LIGO Scientific Collaboration, Classical Quantum Gravity **25**, 114041 (2008).
[2] T. Accadia *et al.*, J. Phys. Conf. Ser. **203**, 012074 (2010); F. Acernese *et al.*, Classical Quantum Gravity **25**, 114045 (2008).
[3] H. Grote and the LIGO Scientific Collaboration, Classical Quantum Gravity **25**, 114043 (2008).
[4] D. Tatsumi *et al.*, Classical Quantum Gravity **24**, S399 (2007).
[5] P. Jaranowski and A. Królak, *Analysis of Gravitational-Wave Data* (Cambridge University Press, Cambridge, 2009).
[6] R. N. McDonough and A. D. Whalen, *Detection of Signals in Noise* (Academic Press, San Diego, 1995), 2nd edition.
[7] P. Jaranowski and A. Królak, Living Rev. Relativity **8**, 3 (2005).
[8] P. Jaranowski, A. Królak, and B. F. Schutz, Phys. Rev. D **58**, 063001 (1998).
[9] P. Jaranowski and A. Królak, Phys. Rev. D **59**, 063003 (1999).
[10] P. Jaranowski and A. Królak, Phys. Rev. D **61**, 062001 (2000).
[11] P. Astone, K. M. Borkowski, P. Jaranowski, and A. Królak, Phys. Rev. D **65**, 042003 (2002).
[12] P. Astone, K. M. Borkowski, P. Jaranowski, M. Pietka, and A. Królak, Phys. Rev. D **82**, 022005 (2010).
[13] P. R. Brady, T. Creighton, C. Cutler, and B. F. Schutz, Phys. Rev. D **57**, 2101 (1998).
[14] P. R. Brady and T. Creighton, Phys. Rev. D **61**, 082001 (2000).
[15] R. Prix and B. Krishnan, Classical Quantum Gravity **26**, 204013 (2009).
[16] P. Jaranowski and A. Królak, Classical Quantum Gravity **27**, 194015 (2010).
[17] B. Abbott *et al.* (LIGO Scientific Collaboration), Phys. Rev. D **69**, 082004 (2004).
[18] B. Abbott *et al.* (LIGO Scientific Collaboration), Phys. Rev. Lett. **94**, 181103 (2005).
[19] B. Abbott *et al.* (LIGO Scientific Collaboration), Phys. Rev. D **76**, 042001 (2007).
[20] B. Abbott *et al.* (LIGO Scientific Collaboration), Astrophys. J. Lett. **683**, L45 (2008).
[21] B. P. Abbott *et al.* (LIGO Scientific Collaboration and Virgo Collaboration), Astrophys. J. **713**, 671 (2010).
[22] C. Messenger, R. Prix, and M. A. Papa, Phys. Rev. D **79**, 104017 (2009).
[23] R. Prix, Classical Quantum Gravity **24**, S481 (2007).
[24] I. W. Harry, B. Allen, and B. S. Sathyaprakash, Phys. Rev. D **80**, 104014 (2009).
[25] G. M. Manca and M. Vallisneri, Phys. Rev. D **81**, 024004 (2010).
[26] Ch. Röver, J. Phys. Conf. Ser. **228**, 012008 (2010).
[27] J. H. Conway and N. J. A. Sloane, *Sphere Packings, Lattices and Groups* (Springer-Verlag, New York, 1999), 3rd edition.